COMMUNICATION

Hierarchical Hollow Spheres of Fe_2O_3@Polyaniline for Lithium Ion Battery Anodes

Jae-Min Jeong, Bong Gill Choi, Soon Chang Lee, Kyoung G. Lee, Sung-Jin Chang, Young-Kyu Han, Young Boo Lee, Hyun Uk Lee, Soonjo Kwon, Gaehang Lee, Chang-Soo Lee,* and Yun Suk Huh**

Lithium ion batteries (LIBs) have mainly been employed as energy sources for portable electronics, and are now expanding their applications to a larger scale, particularly electric vehicles and grid storage.[1–3] Ever increasing demand in such applications has stimulated significant interest in the development of energy storage electrode materials.[4–9] In this context, α-Fe_2O_3 is a non-toxic, low cost material and has a higher theoretical capacity value (1007 mAh g^{-1}) than commercial graphite (372 mAh g^{-1}). Thus, it has been considered as one of the most promising anode candidates.[10–12] Significant capacity fading, however, is still observed at both high rate and long-term charge/discharge cycling due to the large specific volume changes during battery cycling and kinetic limitations of its intrinsic nature.[13,14] The ease of fabrication of electrode materials that can be mass produced at low cost is also of great interest on an industrial scale.

Hierarchical complexity, along with large surface area, a short diffusion length, and good mechanical integrity, has been appealing as an attractive structure for the design and fabrication of electrode materials to overcome the current issues and challenges.[15–18] Recently, Lou et al. synthesized an urchin-like hollow structure of iron oxides and reported their improvement in the cycling life compared to a non-hollow structure.[10,19,20] Despite this previous effort, the rate capability still remains insufficient to fully realize its potential in LIBs due to the intrinsically poor electronic conductivity of iron oxides. Construction of a core-shell structure, particularly carbon coating of the inner- or outer walls of active materials, could be a good approach to increasing the conductivity of the entire electrodes.[21,22] As a consequence, the hierarchical core-shell hollow structure of iron oxide@carbon can be expected to allow not only the efficient and rapid transfer of ion and electron, but also the accommodation of volume expansion during cycling. However, it is still a challenging task to develop a simple and reliable method for hierarchical core-shell hollow structures with a controlled size, morphology, and composition under mass manufacture. Most template-assisted methods for hollow structures often require a complicated experimental procedure of the preparation/removal of templates and suffer from partial structural collapse during the removal of templates.[20,23] The thermal decomposition of carbon precursors, which is used widely for carbon coatings, causes environmental problems because of the formation of volatile organic compounds, CO and CO_2, and sometimes leads to the inferior reconstruction (i.e., structure, size, and phase) of materials.[24,25]

Herein, we developed a simple and scalable approach for the fabrication of hierarchical hollow spheres of Fe_2O_3@polyaniline (PANI) using a template-free method of iron oxides followed by a post PANI coating process. A conducting polymer coating allows us to an efficient approach to improving electron transport in electrodes because of its easy and environmental processability as well as the unique electrical properties of conducting polymers.[25,26] Of particular interest, we found that polymerization of aniline monomers using HCl solution leads to the simultaneous etching of iron oxides and PANI coating process, resulting in the successful formation of heterogeneous and hollow structures of Fe_2O_3@PANI. By using as-prepared composites, we were able to demonstrate their excellent electrochemical characteristics as an anode for LIBs, such as improved large reversible capacity, rate capability, and long-term cycling stability, compared to the urchin-like Fe_2O_3.

J.-M. Jeong,[+] Prof. C.-S. Lee
Department of Chemical Engineering
Chungnam National University
Daejeon, 305–764, Republic of Korea
E-mail: rhadum@cnu.ac.kr
Dr. B. G. Choi,[+][†] Dr. S.-J. Chang, Dr. H. U. Lee, Dr. G. Lee
Division of Materials Science, Korea Basic Science Institute
Daejeon, 305–333, Republic of Korea
E-mail: k1811@kaist.ac.kr
S. C. Lee
Department of Fine Chemical Engineering and Applied Chemistry Chungnam National University
Daejeon, 305–764, Republic of Korea
Dr. K. G. Lee
Department of Chemical Engineering
University of Michigan
Ann Arbor, Michigan, 48109, United States
Prof. Y.-K. Han
Department of Energy and Materials Engineering
Dongguk University-Seoul
Seoul, 100–715, Republic of Korea
Dr. Y. B. Lee
Jeonju Center, Korea Basic Science Institute
Jeonju, 561–180, Republic of Korea
Prof. S. Kwon, Prof. Y. S. Huh
Department of Biological Engineering
Biohybrid Systems Research Center(BSRC)
Inha University
Incheon, 402–751, Republic of Korea
E-mail: yunsuk.huh@inha.ac.kr
[+]These authors contributed equally to this work.
[†]Department of Chemical Engineering, University of Michigan, Ann Arbor, Michigan 48109, United States

DOI: 10.1002/adma.201302710

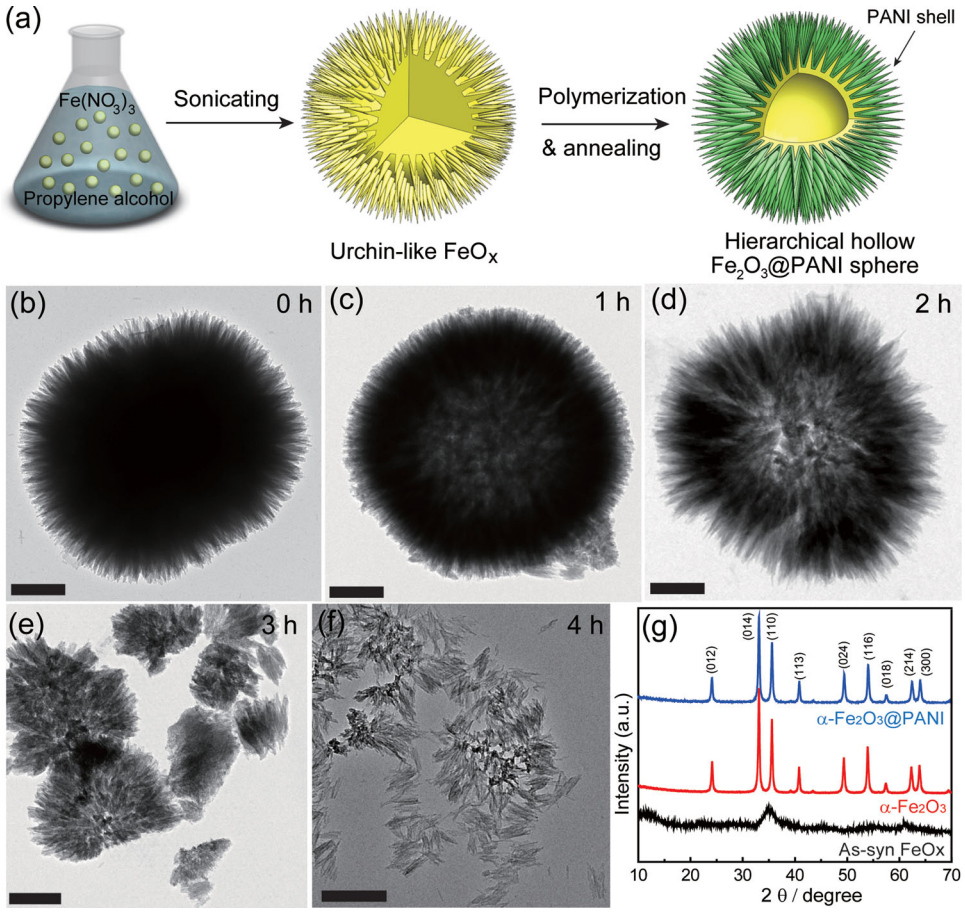

Figure 1. (a) Schematic diagram illustrating the procedure to fabricate hierarchical Fe_2O_3@PANI through simultaneous in- and exterior construction. (b-f) TEM images of the samples obtained from different reaction times during PANI polymerization (Scale bar is 200 nm.). (g) XRD patterns of the as-syn FeO_X, α-Fe_2O_3, and α-Fe_2O_3@PANI.

Overall strategy for production of Fe_2O_3@PANI is schematically depicted in **Figure 1**a. We first developed a template-free sonochemical method for the gram scale synthesis of highly uniform urchin like FeO_X spheres. A typical iron precursor of $Fe(NO_3)_3 \cdot 9H_2O$ (16.16 g 40 mM) was dissolved in a solution of propylene alcohol (40 mL) and then sonicated for 30 min at room temperature. After sonication and washing, 2.8 g of FeO_X spheres was obtained. Scanning electron microscope (SEM) and transmission electron microscope (TEM) images (Supporting Information, Figure S1) show typical urchin-like FeO_X samples, which were spherical in shape with a diameter size of approximately 1 μm. Detailed formation mechanism of urchin-like FeO_X sphere was studied by observing reaction time-dependent morphological evolution (Figure S2). This sonochemical method under mild conditions enabled the simple, rapid, and large scale production of uniform-sized FeO_X spheres without any templates. The heterogeneous and hollow structure of Fe_2O_3@PANI was accomplished by the in-situ polymerization of aniline monomers using FeO_X spheres. For this, aniline monomers were attached to the FeO_X surface by means of electrostatic and hydrogen bonding interactions between them. After removing the unbound aniline monomers, HCl and ammonium persulfate solutions were added to the FeO_X samples dispersed in N-methyl-2-pyrrolidone (NMP) solution. Of particular interest, it was found that the preorganized aniline units were polymerized at the exterior, while the interior etching process occurred simultaneously through the hydrolysis of FeO_X. It should be noted here that HCl was employed as both the dopant for polyaniline and etchant to dissolve iron oxides. In addition, SEM image of some broken samples shows clearly that FeO_X@PANI is hollow and its outer shell is densely packed with submicrometer-sized needles (Figure S3). Finally, annealing was performed at 250 °C under N_2 for the conversion of FeO_X@PANI to Fe_2O_3@PANI. The hierarchical structure was maintained after the thermal treatment (Supporting Information, Figure S4). All X-ray diffraction (XRD) patterns (Figure 1) of the sample indicate the formation of α-Fe_2O_3 with a rhombohedral phase and lattice parameters of a = 0.504 and c = 1.375 nm.[27]

TEM images of Figures 1b–f exhibit morphological changes of Fe_2O_3@PANI spheres for the different reaction times ranging from 0 to 4 h. As the reaction proceeded, iron oxides were etched gradually from non-hollow FeO_X spheres, leaving behind a hollow structure (Figures 1b and 1c). In particular, hierarchical hollow structure clearly appeared at reaction time of 2 h (Figure 1d). When a reaction time was prolonged to 3 h,

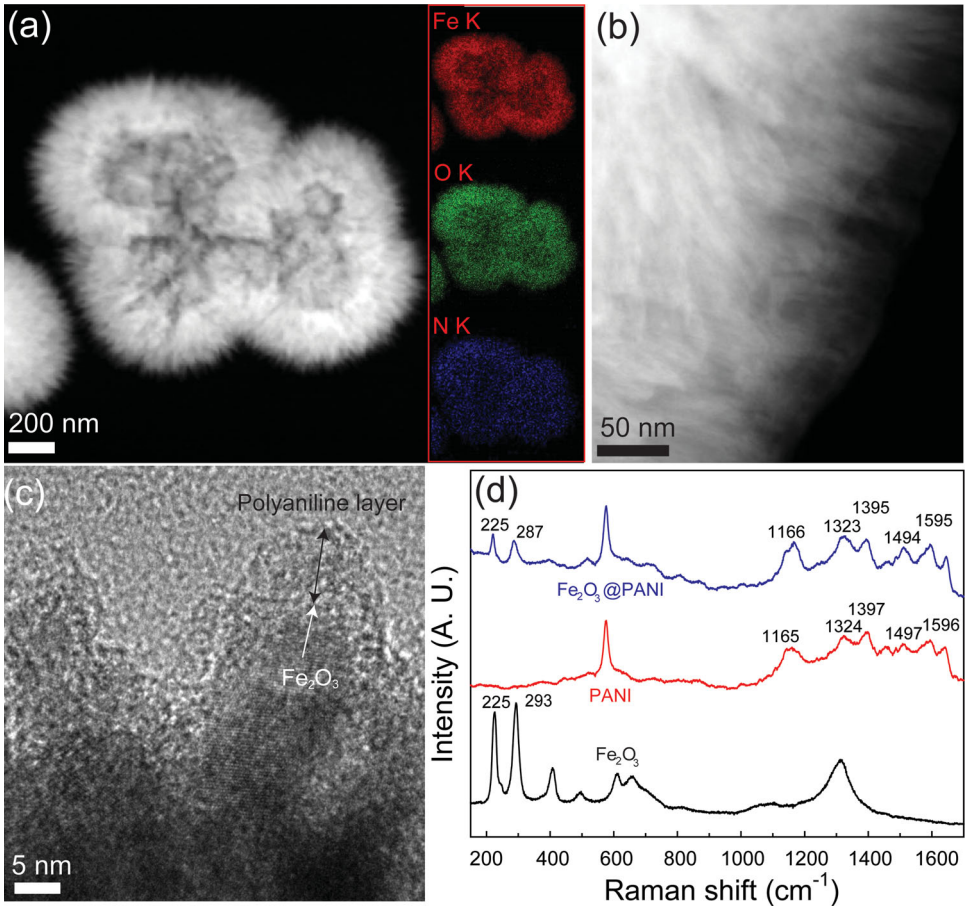

Figure 2. (a) and (b) HADDF-STEM images of Fe_2O_3@PANI (Inset images are EDS mapping of Fe, O, and N according to the image of Figure 2a). (c) HR-TEM image of Fe_2O_3@PANI. (d) Raman spectra of Fe_2O_3, PANI, and Fe_2O_3@PANI.

the structural collapse was observed (Figure 1e). The complete destruction of the hierarchical structure then occurred after a further reaction time above 4 h (Figure 1f). This sequential inner-core etching and successful formation of hollow Fe_2O_3@PANI can be explained through two critical points: polymer protection layer and mixed phase of FeO_X. It has been well known that polymer itself become anti-corrosion layers from acids.[28,29] In this case, PANI is coated over the outermost surface of iron oxide sphere, and thus enables to enhance the resistivity to the acid solution (i.e., HCl). In addition, the mixed phase of FeO_X is another key factor in the formation of a hierarchical hollow structure. In general, the dissolution process using HCl is dependent on the phases of iron, leading to different dissolution rates.[30] The FeO_X samples obtained using the sonochemical method in this work were composed of mixed phases and an amorphous structure (XRD pattern of Figure 1g). Therefore, it could be possible that the formation of hollow structure for FeO_X occurred by the different leaching rates during the HCl etching process. To prove this, we prepared urchin-like Fe_2O_3 samples by an annealing treatment using FeO_X. As expected, one can observe the separated pieces of Fe_2O_3 rather than hollow structures, even after a short etching time of 30 min (Figure S5). Because the morphology of FeO_X depends on the reaction time, we performed Brunauer-Emmett-Teller (BET) analysis in order to evaluate the BET surface areas (Table S1). The Fe_2O_3@PANI obtained at an etching time of 2 h shows a maximum surface area of 236.9 m^2 g^{-1}. The increased surface area compared to the original sample was attributed to the additional generation of inner hierarchical porosity derived from an etching reaction (Figure S6). Therefore, the reaction time of 2 h was determined as the optimal synthetic condition of hierarchical hollow structure because of its high surface area benefit, which is large enough to easily access the electrolyte ions into the internal void spaces.

The core-shell structure of Fe_2O_3@PANI was intensively confirmed by TEM and Raman spectroscopy. As shown in **Figure 2**a and 2b, high-angle annular dark-field scanning TEM (HAADF-STEM) image reveals the urchin-like hollow structure of the Fe_2O_3@PANI. Energy dispersive X-ray (EDS) of the elemental mappings was performed on the sample of Figure 2a. The nitrogen signal for PANI and the oxygen and iron signals for Fe_2O_3 were overlapped uniformly across the entire sample, which is indicative of uniform PANI coating on the Fe_2O_3 surface. In particular, high-resolution TEM (HR-TEM) image of Figure 2c clearly confirmed the key structural characterization of the Fe_2O_3@PANI; core of Fe_2O_3 was coated with the shell of PANI with a thickness of 5 ≈ 10 nm, maintaining the hierarchical structure. In addition, the chemical structure

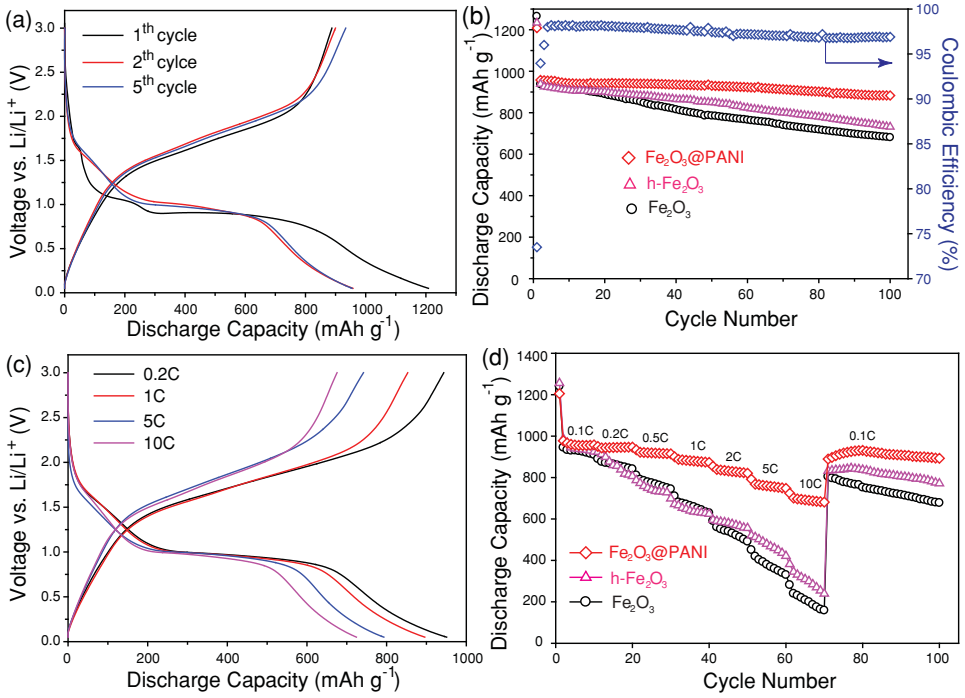

Figure 3. (a) Galvanostatic charge–discharge curves of Fe_2O_3@PANI electrode cycled between 3 and 0.05 V (*vs.* Li^+/Li) at 0.1 C rate (1 C = 1000 mA g^{-1}). (b) Cyclic performance of Fe_2O_3, h-Fe_2O_3, and Fe_2O_3@PANI electrodes at a 0.1 C rate. (c) Galvanostatic charge–discharge curves of Fe_2O_3@PANI electrode at different cycling rates. (d) Rate capability of Fe_2O_3, h-Fe_2O_3, and Fe_2O_3@PANI electrodes at different rates ranging from 0.1 C to 10 C.

of the Fe_2O_3@PANI sphere was investigated using Raman spectroscopy, as shown in Figure 2d. Newly appeared peaks at 1165 cm^{-1} (C–H bending of benzenoid rings), 1494 cm^{-1} (C = N stretching of the quinoid ring), and 1595 cm^{-1} (C–C stretching of the benzenoid rings) for Fe_2O_3@PANI clearly indicates the presence of PANI compared to the bare Fe_2O_3.[31,32] In addition, two distinct peaks, 1323 and 1395 cm^{-1}, were assigned to the stretching vibrations of C–N^+ fragments, indicating the emeraldine salt of PANI, which is a highly electrical conductive form.[31] Comparing to the bands of pure Fe_2O_3 and polyaniline, the bands of Fe_2O_3@PANI in the composite structure broadened and shifted. This might be attributed to the strong mutual interactions of hydrogen bonding between the Fe–O of Fe_2O_3 and NH group of PANI.[33] The weight fraction of PANI in the composites was calculated from elemental analysis, giving a value of ≈10 wt%.

We next demonstrated the ability of Fe_2O_3@PANI as anode material for LIBs. The electrochemical performance was evaluated by preparing coin-type half cells that employ Fe_2O_3@PANI as a working electrode and Li foil as a counter/reference electrode. In order to clearly demonstrate superior features of Fe_2O_3@PANI on electrochemical performance, two control samples, (1) urchin-like Fe_2O_3 without etching and PANI coating and (2) urchin-like hollow Fe_2O_3 (h-Fe_2O_3) without PANI coating, were also tested. Detailed preparation of these control samples was described in Experimental section. **Figure 3**a shows the galvanostatic charge/discharge curves of the Fe_2O_3@PANI electrode at rate of 0.1 C (1 C = 1000 mAh g^{-1}) in the voltage range of 0.05–3 V (versus Li^+/Li). Upon this galvanostatic cycling, the initial discharge and charge capacities of the Fe_2O_3@PANI electrode were as high as 1208 and 958 mAh g^{-1} with a 73.5% Coulombic efficiency. This initial low Coulombic efficiency is related to the solid electrolyte interphase layer accompanying the electrolyte decomposition.[34] This showed a rapid increase to 96% after the second cycle, which was then stabilized to 98% over 100 cycles. Figure 3b shows the cycling performance of the Fe_2O_3@PANI electrode at a constant current rate at 0.1 C up to 100 cycles. As expected, Fe_2O_3@PANI electrode showed good cycling performance; the initial capacity decreased slightly to 893 mAh g^{-1} even after 100 cycles of charge/discharge. By contrast, during a few cycles, a rapid decay of capacity was observed in the non-hollow Fe_2O_3 electrode and the initial capacity showed a continuous decrease to 680 mAh g^{-1}, while h-Fe_2O_3 electrode exhibited 732 mAh g^{-1} after 100 cycles (Figure 3b). Such capacity retention was examined further by increasing the charge/discharge rates from 0.1 C to 10 C. As shown in Figure 3c, when increasing the cycling rates, Fe_2O_3@PANI exhibited decent capacity retention: 950 mAh g^{-1} (0.2 C), 856 mAh g^{-1} (1 C), 793 mAh g^{-1} (5 C), and 724 mAh g^{-1} (10 C). The obtained capacities were plotted, as shown in Figure 3d, along with the applied current densities. Upon all of the current densities, Fe_2O_3@PANI showed continuously higher capacities than those of non-hollow Fe_2O_3 and h-Fe_2O_3 electrodes (Figure 3d), which is indicative of the superior rate capability for Fe_2O_3@PANI. Remarkably, this remaining capacity of 681 mAh g^{-1} when cycled at a high rate of 10 C was still higher than the theoretical capacity of graphite (372 mAh g^{-1}) and is also higher than those of other reported iron oxide-based materials

even at a lower rate, including spindle-like mesoporous Fe_2O_3,[34] Fe_2O_3/carbon composites,[23] and Fe_2O_3/graphene composites.[35]

An electrochemical impedance spectroscopy (EIS) measurement was performed in order to deeply understand the merits of the Fe_2O_3@PANI electrode compared to the bare Fe_2O_3 electrode. The Nyquist plots for the samples are shown in Figure S7 with a frequency range of 100 kHz to 0.01 Hz. The diameter of the semi-circle at the high frequency was dramatically decreased in Fe_2O_3@PANI sample, compared to the Fe_2O_3, indicating the enhanced charge transfer. This is strongly attributed to the increased contact area at the electrode/electrolyte interface as well as the enhanced electrical conductivity of the overall electrode.[36] It is noteworthy that the core-shell hollow structure of Fe_2O_3@PANI is critical factor for facilitating charge transfer process. At the low frequency region, a more vertical straight line of the Fe_2O_3@PANI compared to the Fe_2O_3 is further evident for the faster Li^+ ion diffusion behavior of the Fe_2O_3@PANI electrode. Once again, we emphasized the unique structure of Fe_2O_3@PANI on major contribution to the enhanced cycling and rate performances compared to bare Fe_2O_3 and hollow Fe_2O_3. The porous nature can provide largely available charge storage sites with rapid ionic pathways, while accommodating large volume exchange. In addition, the PANI coating enables an increase in the electrical conductivity of the entire electrodes.

In conclusion, we have developed a hierarchical core-shell hollow structure of Fe_2O_3@PANI through a simple and scalable manner for LIB anodes that yield robust electrochemical performances. Such a core-shell hollow structure has been accomplished by a simultaneous etching and polymerization processes using urchin-like iron oxide spheres. The unique structure was important; therefore, we optimized it by simple control of the reaction time. Consequently, the well-defined Fe_2O_3@PANI provided efficient and rapid ion/electron pathways for electrochemical reactions. When testing the LIB anode, Fe_2O_3@PANI showed a large reversible capacity, high rate capability, and excellent cycling stability during 100 cycles. The simple and scalable route for Fe_2O_3@PANI developed in this study can be readily applied to a wide range of electrochemical devices where charge transport might impede the development of high performance devices.

Experimental Section

Synthesis of urchin-like iron oxides: Samples were prepared using a template-free sonochemical method according to the following procedures. First, $Fe(NO_3)_3{\cdot}9H_2O$ (16.16 g, Sigma-Aldrich) was dispersed in propylene alcohol (40 mL) in a 50 mL beaker, and was then irradiated by ultrasound with a frequency of 20 kHz. After a reaction time of 30 min, the resulting sample was then cooled to room temperature (RT). The products were filtered and washed several times with water and ethanol solutions. Finally, a solid powder was obtained by drying overnight at 60 °C under vacuum.

Synthesis of hierarchical hollow Fe_2O_3@PANI: Fe_2O_3@PANI was obtained using simultaneous one-step of in-situ polymerization and chemical etching process in the same reactor. Prior to this, the above prepared FeO_X powder (2.8 g) was dispersed in NMP solution (50 mL). An aniline monomer solution (10 mM) was added and the mixture was stirred at RT for 12 hours. The resulting mixture was washed to remove the unbound aniline monomers. The aniline-functionalized FeO_X samples were re-dispersed in NMP solution, followed by the addition of ammonium persulfate (0.1 g) and HCl (0.1 M, 10 mL) solution. Subsequently, the mixture was placed on a magnetic stirrer at RT for 1–4 h. During this reaction, Fe ions were released by a hydrolysis reaction. The final products were collected by filtration, and washed several times with water and ethanol solutions. These samples were then annealed at 250 °C for 4 hours to achieve clear transfer into the Fe_2O_3 phase. As control samples, non-hollow Fe_2O_3 and hollow Fe_2O_3 (h-Fe_2O_3) were also prepared. Non-hollow Fe_2O_3 was prepared by annealing the FeO_X obtained from sonochemical synthesis at 250 °C for 4 hours. In addition, h-Fe_2O_3 was obtained using etching process without PANI coating. All the as-obtained samples was dried and stored at 60 °C under vacuum.

Structural characterization: TEM, HAADF-STEM and elemental mapping were performed using a JEM-2200FS microscope at 200 kV. XRD was performed on a Rigaku D/max IIIC (3 kW) with a θ/θ goniometer equipped with a CuKα radiation generator. The XPS data was collected on a Thermo MultiLab 2000 system with an Al Mga X-ray source. The N_2 adsorption/desorption was determined by BET measurements using an ASAP-2010 surface area analyzer. The Raman spectra were measured using a NTEGRA Spectra spectrometer (NT-MDT, Russia).

Electrochemical characterization: The electrochemical measurements were performed using a CR2016 type coin cell with Li metal as the counter/reference electrode, Fe_2O_3@PANI as the working electrode, and 1 M $LiPF_6$ dissolved in ethylene carbonate/dimethyl carbonate/diethyl carbonate (1:2:1 v/v) as the electrolyte. Cu foil was used for the electrical connection to the Fe_2O_3@PANI nanocomposites. The working electrodes were prepared by mixing the Fe_2O_3@PANI nanocomposites (80 wt%), conducting carbon black (10 wt%), and polyvinylidene fluoride binder (10 wt%) in NMP. The cells were assembled in a glove box filled with argon. Galvanostatic charge–discharge cycles were tested using a Wonatech automatic battery cycler at various current densities between 3 and 0.05 V vs. Li^+/Li at room temperature.

Supporting Information

Supporting Information is available from the Wiley Online Library or from the author.

Acknowledgements

We acknowledge the financial support by the National Research Foundation of Korea Grant funded by the Korean Government (MEST, NRF-2010-C1AAA001–0029018) to Y. S. H. This work was also supported by the Gyeongbuk Science & Technology Promotion Center(GBSP) grant funded by the Korea government (KMEST) (KMEST, GBSP-001–111228–003).

Received: June 13, 2013
Revised: July 13, 2013
Published online: August 21, 2013

[1] A. Yoshino, *Angew. Chem. Int. Ed.* **2012**, *51*, 5798.
[2] P. G. Bruce, S. A. Freunberger, L. J. Hardwick, J.-M. Tarascon, *Nat. Mater.* **2012**, *11*, 19.
[3] B. Dunn, H. Kamath, J.-M. Tarascon, *Science* **2011**, *334*, 928.
[4] H. B. Wu, J. S. Chen, H. H. Hng, X. W. Lou, *Nanoscale* **2012**, *4*, 2526.
[5] P. G. Bruce, B. Scrosati, J.-M. Tarascon, *Angew. Chem. Int. Ed.* **2008**, *47*, 2930.
[6] A. S. Aricó, P. Bruce, B. Scrosati, J.-M. Tarascon, W. V. Schalkwijk, *Nat. Mater.* **2005**, *4*, 366.

[7] H. Wu, G. Chan, J. W. Choi, I. Ryu, Y. Yao, M. T. McDowell, S. W. Lee, A. Jackson, Y. Yang, L. Hu, Y. Cui, *Nat. Nanotechnol.* **2012**, *7*, 310.
[8] X. Xin, X. Zhou, J. Wu, X. Yao, Z. Liu, *ACS Nano* **2012**, *6*, 11035.
[9] C. Xu, Y. Zeng, X. Rui, N. Xiao, J. Zhu, W. Zhang, J. Chen, W. Liu, H. Tan, H. H. Hng, Q. Yan, *ACS Nano* **2012**, *6*, 4713.
[10] B. Wang, J. S. Chen, X. W. Lou, *J. Mater. Chem.* **2012**, *22*, 9466.
[11] Z. Wang, L. Zhou, X. W. Lou, *Adv. Mater.* **2012**, *24*, 1903.
[12] B. Koo, H. Xiong, M. D. Slater, V. B. Prakapenka, M. Balasubramanian, P. Podsiadlo, C. S. Johnson, T. Rajh, E. V. Shevchenko, *Nano Lett.* **2012**, *12*, 2429.
[13] N.-S. Choi, Z. Chen, S. A. Freunberger, X. Ji, Y.-K. Sun, K. Amine, G. Yushin, L. F. Nazar, J. Cho, P. G. Bruce, *Angew. Chem. Int. Ed.* **2012**, *51*, 9994.
[14] R. Liu, J. Duay, S. B. Lee, *Chem. Commun.* **2011**, *47*, 1384.
[15] A. Magasinski, P. Dixon, B. Hertzberg, A. Kvit, J. Ayala, G. Yushin, *Nat. Mater.* **2010**, *9*, 353.
[16] B. G. Choi, Y. S. Huh, W. H. Hong, D. Erickson, H. S. Park, *Nanoscale* **2013**, *5*, 3976.
[17] J. Duay, S. A. Sherrill, Z. Gui, E. Gillette, S. B. Lee, *ACS Nano* **2013**, *7*, 1200.
[18] D. S. Jung, T. H. Hwang, S. B. Park, J. W. Choi, *Nano Lett.* **2013**, *13*, 2092.
[19] B. Wang, J. S. Chen, H. B. Wu, Z. Wang, X. W. Lou, *J. Am. Chem. Soc.* **2011**, *133*, 17146.
[20] B. Wang, H. B. Wu, L. Zhang, X. W. Lou, *Angew. Chem. Int. Ed.* **2013**, *52*, 4165.
[21] A. L. M. Reddy, S. R. Gowda, M. M. Shaijumon, P. M. Ajayan, *Adv. Mater.* **2012**, *24*, 5045.
[22] C. Liu, F. Li, L.-P. Ma, H.-M. Cheng, *Adv. Mater.* **2010**, *22*, E28.
[23] J. E. Lee, S.-H. Yu, D. J. Lee, D.-C. Lee, S. I. Han, Y.-E. Sung, T. Hyeon, *Energy Environ. Sci.* **2012**, *5*, 9528.
[24] Y. Wang, Y. Wang, E. Hosono, K. Wang, H. Zhou, *Angew. Chem. Int. Ed.* **2008**, *47*, 7461.
[25] D. Lepage, C. Michot, G. Liang, M. Gauthier, S. B. Schougaard, *Angew. Chem. Int. Ed.* **2011**, *50*, 6884.
[26] Y. Jung, N. Singh, K.-S. Choi, *Angew. Chem. Int. Ed.* **2009**, *48*, 8331.
[27] G. Sun, B. Dong, M. Cao, B. Wei, C. Hu, *Chem. Mater.* **2011**, *23*, 1587.
[28] C. L. Zhu, S. W. Chou, S. F. He, W. N. Liao, C. C. Chen, *Nanotechnology* **2007**, *18*, 275604.
[29] X. W. Lou, L. A. Archer, Z. Yang, *Adv. Mater.* **2008**, *20*, 3987.
[30] P. S. Sidhu, R. J. Gilkes, R. M. Cornell, A. M. Posner, J. P. Quirk, *Clays Clay Miner.* **1981**, *29*, 269.
[31] A. Drury, S. Chaure, M. Kröll, V. Nicolosi, N. Chaure, W. J. Blau, *Chem. Mater.* **2007**, *19*, 4252.
[32] Q. Yao, L. Chen, W. Zhang, S. Liufu, X. Chen, *ACS Nano* **2010**, *4*, 2445.
[33] S. S. Umare, B. H. Shambharkar, *J. Appl. Polym. Sci.* **2013**, *127*, 3349.
[34] X. Xu, R. Cao, S. Jeong, J. Cho, *Nano Lett.* **2012**, *12*, 4988.
[35] J. Qu, Y.-X. Yin, Y.-Q. Wang, Y. Yan, Y.-G. Guo, W.-G. Song, *ACS Appl. Mater. Interfaces* **2013**, *5*, 3932.
[36] B. G. Choi, M. Yang, W. H. Hong, J. W. Choi, Y. S. Huh, *ACS Nano* **2012**, *6*, 4020.